Journal of Power Sources 271 (2014) 187–194

Contents lists available at ScienceDirect

Journal of Power Sources

journal homepage: www.elsevier.com/locate/jpowsour

$La_{0.8}Sr_{0.2}Fe_{0.8}Cu_{0.2}O_{3-\delta}$ as "cobalt-free" cathode for $La_{0.8}Sr_{0.2}Ga_{0.8}Mg_{0.2}O_{3-\delta}$ electrolyte

Francesca Zurlo [a], Elisabetta Di Bartolomeo [a, *], Alessandra D'Epifanio [a], Valeria Felice [b], Isabella Natali Sora [b], Luca Tortora [c], Silvia Licoccia [a]

[a] Department of Chemical Science and Technologies & NAST Center University of Rome Tor Vergata, Via della Ricerca Scientifica, 00133 Rome, Italy
[b] INSTM R.U. and Department of Engineering, University of Bergamo, Dalmine, BG I-24044, Italy
[c] Department of Physics and Mathematics, Surface Analysis Laboratory, University Roma Tre, Via della Vasca Navale 84, 00146 Rome, Italy

HIGHLIGHTS

- Synthesis and characterization of $La_{0.8}Sr_{0.2}Fe_{0.8}Cu_{0.2}O_{3-\delta}$ (LSFCu).
- Chemical compatibility with $La_{0.8}Sr_{0.2}Ga_{0.8}Mg_{0.2}O_{3-\delta}$ (LSGM) is investigated.
- Electrical and electrochemical performance of LSFCu are measured.
- Single cells with LSFCu and $La_{0.6}Sr_{0.4}Fe_{0.8}Co_{0.2}O_{3-\delta}$ (LSFCo) are similar.

GRAPHICAL ABSTRACT

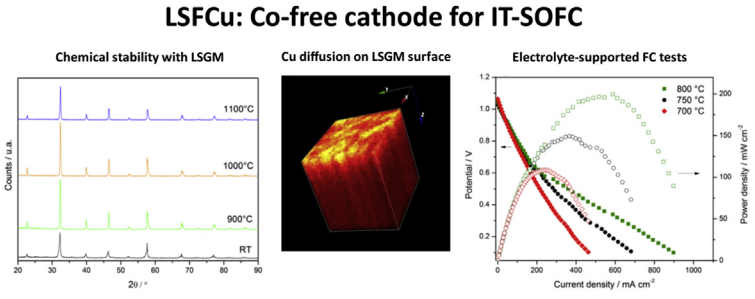

ARTICLE INFO

Article history:
Received 30 April 2014
Received in revised form
11 July 2014
Accepted 30 July 2014
Available online 6 August 2014

Keywords:
SOFC
Cathode
Perovskite structure
LSGM electrolyte

ABSTRACT

A "cobalt-free" cathode material with stoichiometric composition $La_{0.8}Sr_{0.2}Fe_{0.8}Cu_{0.2}O_{3-\delta}$ (LSFCu) was specifically developed for use with $La_{0.8}Sr_{0.2}Ga_{0.8}Mg_{0.2}O_{3-\delta}$ (LSGM) electrolyte in intermediate temperature solid oxide fuel cell (IT-SOFC) systems. The chemical stability of LSFCu in contact with LSGM electrolyte was investigated by structural and morphological analysis. The electrochemical properties of LSFCu dense pellets were investigated in the temperature range 600–750 °C by electrochemical impedance spectroscopy (EIS). LSFCu|LSGM|LSFCu symmetrical cells were prepared and area specific resistance (ASR) values, directly depending on the rate limiting step of the oxygen reduction reaction, were evaluated. Fuel cells were prepared using LSFCu as cathode material on a LSGM pellet and electrochemical tests were performed in the 700–800 °C temperature range and compared to similar fuel cells prepared by using commercial $La_{0.6}Sr_{0.4}Fe_{0.8}Co_{0.2}O_{3-\delta}$ (LSFCo) as a cathode. The maximum current density and power density recorded for LSFCu and LSFCo were similar. This fact demonstrates that Cu can be used as Co substitute in perovskite cathode materials.

1. Introduction

Most materials that have been investigated for application as cathodes in solid oxide fuel cells (SOFCs) show a perovskite structure (ABO_3) [1–3] Sr-doped $LaMnO_3$ and related materials are suitable for high temperature SOFCs, while more electrochemically/catalytically active alternative cathode materials are needed for the Intermediate Temperature (IT) range (500–750 °C). Cobalt containing oxides of different composition, such as $La_{1-x}Sr_xMn_{1-y}Co_yO_{3-\delta}$ (LSCM) [4], $La_{1-x}Sr_xFe_{1-y}Co_yO_{3-\delta}$ (LSFCo) [5–7] and $Ba_{1-x}Sr_xFe_{1-y}Co_yO_{3-\delta}$ (BSCF) [8,9] have been investigated and they all possess the needed requirements for cathode

* Corresponding author. Tel.: +39 0672594491; fax: +39 0672594328.
E-mail address: dibartolomeo@uniroma2.it (E. Di Bartolomeo).

http://dx.doi.org/10.1016/j.jpowsour.2014.07.183
0378-7753/

materials, i.e. mixed ionic–electronic conductivity, with electronic conductivity as high as 100 S cm^{-1}, and good catalytic activity for oxygen reduction reaction (ORR) but most of these materials lack proper chemical stability [5–9]. Insufficient chemical compatibility with the electrolyte, high cost of compositional elements, and easy evaporation are among other issues preventing the use of cobalt containing oxides for practical long-term applications.

$La_{0.8}Sr_{0.2}Ga_{0.8}Mg_{0.2}O_{3-\delta}$ (LSGM) [10,11] is considered among the most promising electrolytes for IT-SOFCs because of its very large ionic conductivity (ca. 0.02 S cm^{-1} at 600 °C) [12], although the formation of insulating secondary phases and cations interdiffusion across the interface with electrodic layers have been often observed [13–15,1]. The problem of diffusivity and the formation of solid solutions at the interface with the investigated LSFCo cathode material has been previously described in the literature [16,17]. Sakai et al. [13] demonstrated the Co and Fe diffusivities in LSGM and concomitant Mg and Ga diffusivities in LSFCo. Moreover, the thermal expansion mismatch between LSFCo cathode and LSGM electrolyte may lead to insufficient contact points and thus to the detachment of cathode layers, which limits the application of cobalt containing cathode materials.

With the aim of developing a performing and stable cathode material for LSGM-based IT-SOFCs, a novel "cobalt-free" perovskite oxide $La_{0.8}Sr_{0.2}Fe_{0.8}Cu_{0.2}O_{3-\delta}$ (LSFCu) was investigated.

The feasibility of LSFCu as cathode material for IT-SOFCs has been demonstrated on the basis of structural, thermal, and electrochemical studies [18–20]. The material has been tested with different electrolytes such as GDC [21] and YSZ [22]. Cell performance in the presence of SDC electrolyte has also been reported by Zhou et al. [23].

In this work, the oxide stoichiometry, $La_{0.8}Sr_{0.2}Fe_{0.8}Cu_{0.2}O_{3-\delta}$, was chosen to minimize cation diffusion at the interface with the most performing electrolyte $La_{0.8}Sr_{0.2}Ga_{0.8}Mg_{0.2}O_{3-\delta}$: the cation molar ratio in both the A and B sites is the same of the electrolyte material. The structural and chemical compatibility was investigated at different temperatures, electrochemical performances of LSFCu|LSGM|LSFCu symmetrical cells and fuel cell tests are discussed and compared to the electrochemical performances of similar cells with $La_{0.6}Sr_{0.4}Fe_{0.8}Co_{0.2}O_{3-\delta}$ (LSFCo) cathode material.

2. Experimental

$La_{0.8}Sr_{0.2}Fe_{0.8}Cu_{0.2}O_{3-\delta}$ powders were prepared by citrate autocombustion of dry gel obtained from a solution of the corresponding nitrates into citric acid solution as previously reported [20]. The resulting light weight powder was heated to 600 °C for 3 h in air to remove organic residues, obtaining a black powder. Commercial LSGM and LSFCo were supplied by Praxair. To investigate LSFCu chemical compatibility with LSGM, a mixture of the two oxide powders (1:1 wt) was heated to 900, 1000 and 1100 °C for 4 h in air and investigated by X-ray powder diffraction using a Philips X-Pert Pro 500 diffractometer. Dense electrolyte pellets of LSGM were obtained by mixing the powder with 5 wt% polyvinylpyrrolidone (PVP) as binder, uniaxially pressed at 740 MPa and sintered at 1500 °C for 10 h in air. Pellets were approximately 0.5 mm thick and with a relative density of 99.8%. Pellets of doped lanthanum ferrites were uniaxially pressed at 200 MPa and sintered at 1250 °C for 4 h.

To examine the cations diffusivity at the electrode|electrolyte interface and their elemental distribution changes on the surface of LSGM pellets, diffusion couples of dense polycrystals with surface slightly polished with abrasive paper were prepared attaching in couples: LSGM|LSFCu and LSGM|LSFCo bound with Pt wires and heat treated at 1100 °C for 4 h. The elemental distribution in the vicinity of LSGM interface was analyzed by time of flight secondary ion mass spectrometry (ToF-SIMS, TOF.SIMS[5], IONTOF GmbH, Münster, Germany). ToF-SIMS experiments were performed by using a 30 keV Bi^+ liquid metal ion gun (LMIG) primary ion beam and a 1 keV Cs^+ second ion gun for sputtering. Sputtering was performed by rastering over a 300 μm square region. Analysis was done on the central area (100 × 100 μm) of the sputtered region. A low energy electron flood gun was activated to neutralize any residual charge on the surface of the sample. A stylus profilometer (P7, KLA-Tencor, San Jose, CA) was used to measure the depth z of the SIMS craters after sputtering each sample for a fixed time t.

Microstructural and chemical analysis of pellets was carried out by using a field emission scanning electron microscope (FE-SEM, SUPRA™ 35, Carl Zeiss SMT, Oberkochen, Germany). and energy dispersive microanalysis (EDX, INCAx-sight, Model: 7426, Oxford Instruments, Abingdon, Oxfordshire, UK).

The electrical conductivity of LSFCu pellets (diameter of 11 mm) was measured from 350 to 750 °C in synthetic air with a standard four-probe DC method and compared to LSFCo conductivity. The probes were placed in a linear configuration with a 2 mm tip spacing and gold was used for contacts and wires.

To investigate the electrochemical behavior, LSFCu|LSGM|LSFCu symmetric cells were prepared. LSFCu powders mixed with a commercial screen printing oil (Sigma–Aldrich, α-Terpineol ≥96% diluted with toluene) were painted on both sides of LSGM dense pellets (thickness of 0.5 mm and diameter of 12 mm), dried and fired at 900 °C for 2 h. Electrodes (diameter of 8 mm) were covered with a diluted Au paste (Heraeus, C5755A) to obtain a uniform and porous current collector. For comparison, LSFCo|LSGM|LSFCo symmetric cells were prepared likewise and tested. A microstructural analysis of electrolyte|cathode interfaces was performed using a FE-SEM.

Electrochemical impedance spectroscopy (EIS) measurements were carried out in the 600–750 °C temperature range using a frequency response analyzer (FRA, Solartron 1260), coupled with a dielectric interface (Solartron 1296), in a frequency range between 0.1 Hz and 1 MHz with an AC voltage amplitude of 100 mV.

Electrolyte supported fuel cells were prepared by using a Ni-modified perovskite anode consisting of 70 wt% Ni-perovskite catalyst (10 wt% of Ni impregnated on LSFCo, Praxair) and 30 wt% $Ce_{0.9}Gd_{0.1}O_2$ (CGO, Praxair) as reported in the literature [24,25] and LSFCu or LSFCo as cathodes. The single cells were fabricated likewise the symmetric ones. Hydrogen–air fuel cell experiments with cathode exposed to static air and anode to 100 cm^3 min^{-1} of H_2 were carried out at 700, 750 and 800 °C. Electrochemical tests were performed using a potentiostat/galvanostat/FRA PARSTAT 2273.

3. Results and discussion

Fig. 1a and b shows the XRD patterns of LSFCu both pellet and powder and the SEM micrograph of LSFCu pellet sintered at 1250 °C. A perovskite structure consisting of an orthorhombic phase (JCPS: 37-1493) was revealed by XRD patterns, in accordance with what previously reported [20]. The average crystallite sizes, estimated from Scherrer equation, were 18 nm for the powder and 55 nm for the pellet, respectively. The BET surface area of the starting powders was 25 m^2 g^{-1} as reported in Ref. [26]. A dense microstructure is shown by SEM analysis confirming that 1250 °C is a proper sintering temperature.

Fig. 2 shows the XRD patterns of LSFCu and LSGM mixture (1:1 weight ratio) before and after annealing subsequently at 900, 1000 and 1100 °C for 4 h in air. XRD patterns can be indexed by a perovskite orthorhombic structure and no reaction products were detected. However, it was observed that the annealing produced modification in the XRD pattern. Increasing the temperature of the heat treatment caused a slight peak shift toward higher angles

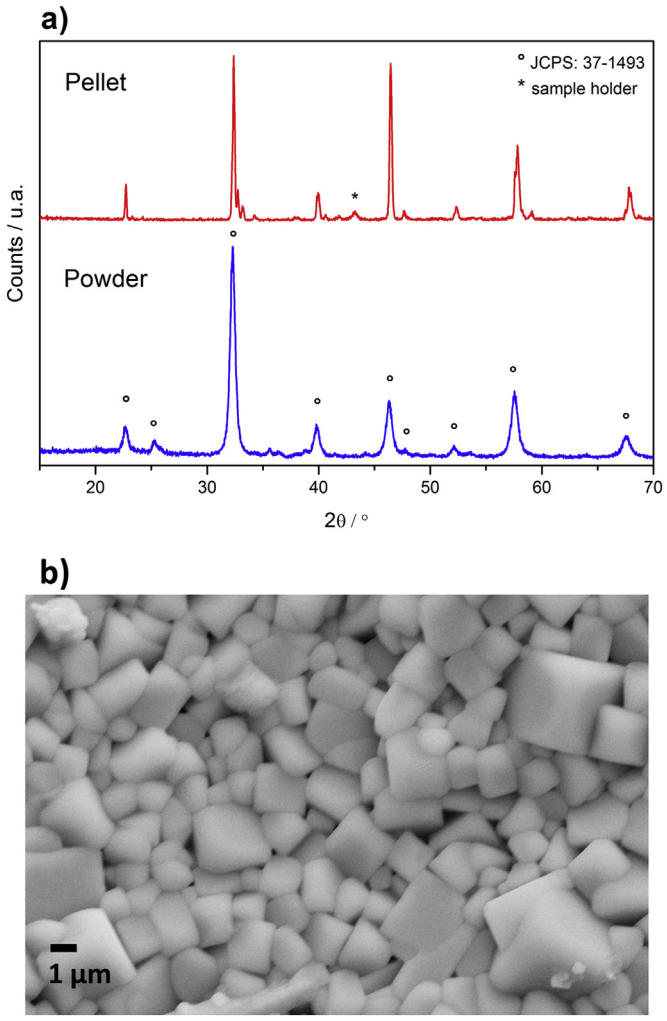

Fig. 1. a) XRD patterns of LSFCu powder and pellet, b) SEM micrograph of LSFCu pellet.

($\Delta 2\theta < 0.05°$) as highlighted in Fig. 2a and a peak broadening around $2\theta = 57–58°$ (Fig. 2b). Coalescence of the two peaks was observed for the sample heated at 1100 °C (Fig. 2b). These features may be explained with the occurrence of cations interdiffusion between LSGM and LSFCu causing the formation of a solid solution with a consequent reduction of the cell volume.

To further investigate the surface cation diffusivity, coupled LSGM and LSFCu pellets were treated at 1100 °C, then the LSFCu layer was removed and SIMS surface analysis of the LSGM pellet was performed. The depth profile of cations is shown in Fig. 3a, while Fig. 3b shows the three-dimensional image of Cu cation surface distribution. As shown in Fig. 3a the SIMS signal intensity of Cu^+ decreases during the first stage of bombardment before reaching a low steady state level after 250 nm from the surface. The 3D image confirms the presence of Cu^+ mainly on the LSGM shallow surface. The intensity of Fe^+ signal is almost constant within all the sputtered material. SIMS analysis was also performed on an LSGM pellet after the same heat treatment, the only difference being the substitution of LSFCu with LSFCo. The two pellets profilometry measurements indicated that the depth of the crater is approximately 1750 nm. Assuming that the sputtering rate $z = dz/dt$ is constant, the sputtering time t can be replaced by the depth z. Fig. 4 shows the comparison of the Cu^+ and Co^+ depth profiles in the two samples normalized with the Ga^+ signal (intensity ratio $I(X)/I(Ga^+)$ with X = Co^+, Cu^+). While the Cu^+ profile intensity

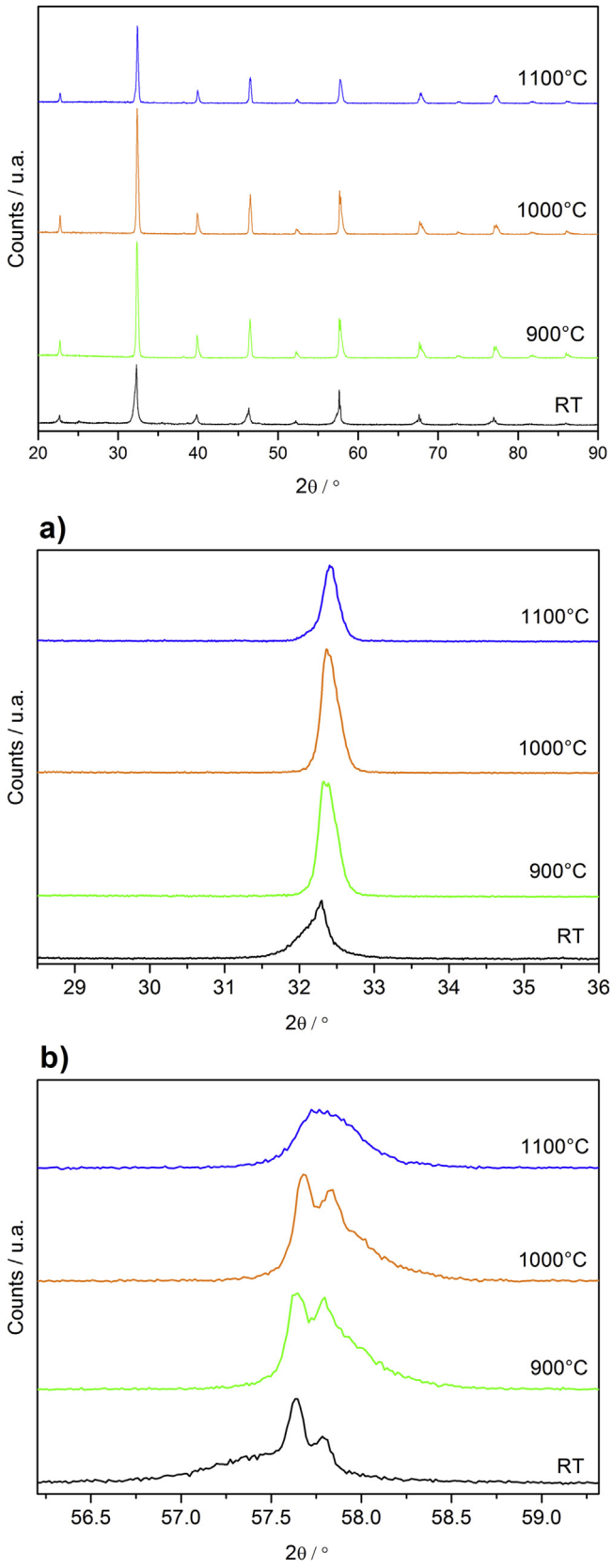

Fig. 2. XRD patterns of LSFCu and LSGM powder mixture before and after annealing at 900, 1000 and 1100 °C for 4 h in air. On the right enlargements around $2\theta = 32°$ (a) and $2\theta = 57–58°$ (b).

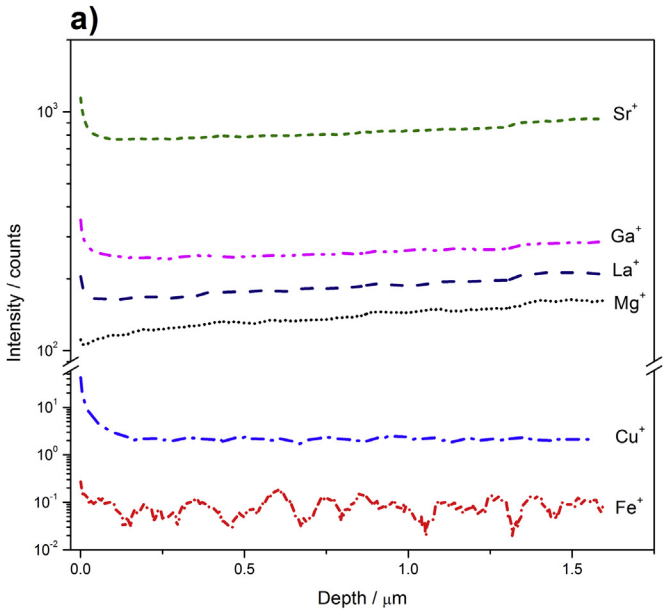

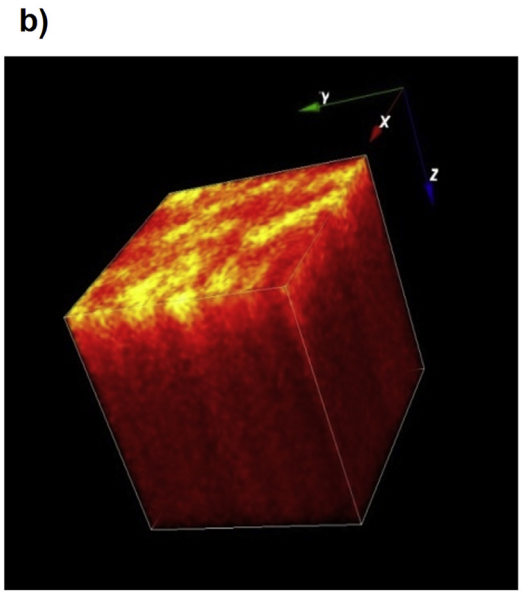

Fig. 3. a) SIMS depth profile of LSGM surface coupled with LSFCu and annealed at 1100 °C for 4 h. (b) Three dimensional distribution of Cu^+ ion in vicinity of LSGM surface.

quickly decreases within 200 nm of the surface, a slight negative drift of the Co^+ profile was revealed within LSGM, confirming the results previously observed by Sakai et al. [13] and indicating a large diffusion of Co^+ in the LSGM matrix.

Fig. 5a and b shows EDX maps with Cu and Co elemental distribution on LSGM surface pellets coupled with LSFCu and LSFCo, respectively. The LSFCo/LSGM diffusion couple was easily disassembled, more difficult was to put the apart in the case of LSFCu/LSGM. Some micrometric parts of LSFCu, preferably in the form of sticks, were stacked on the surface modifying dramatically the LSGM microstructure, thus, the two microstructures appear rather different. In the presence of LSFCu the LSGM microstructure is affected on the surface both at grains and grain boundaries, whereas diffusion of Co is observed mainly at the grain boundaries and the LSGM microstructure is clearly visible. Chemical analysis

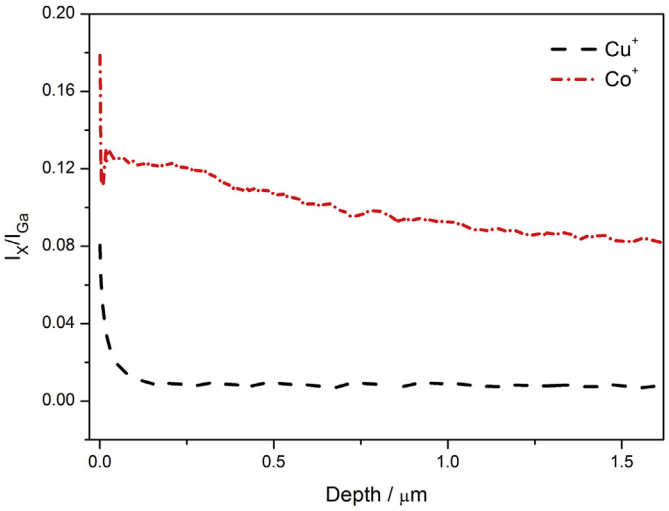

Fig. 4. SIMS depth profiles of LSGM surface: Cu and Co intensities normalized with Ga signal (intensity ratio $I(X)/I(Ga^+)$ with $X = Co^+, Cu^+$).

confirmed that copper is homogeneously distributed on the LSGM surface (Fig. 5a), while the cobalt distribution is preferentially at the grain boundaries as highlighted by the Co map (Fig. 5b), in agreement with the literature [13].

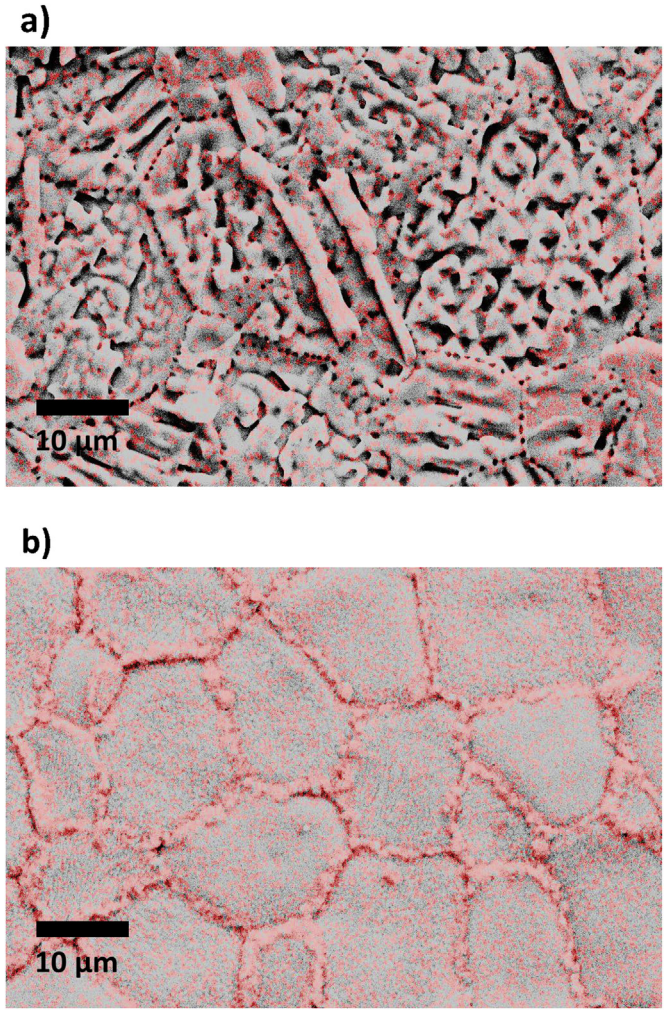

Fig. 5. EDX maps of LSGM surface coupled with LSFCu and LSFCo at 1100 °C for 4 h.

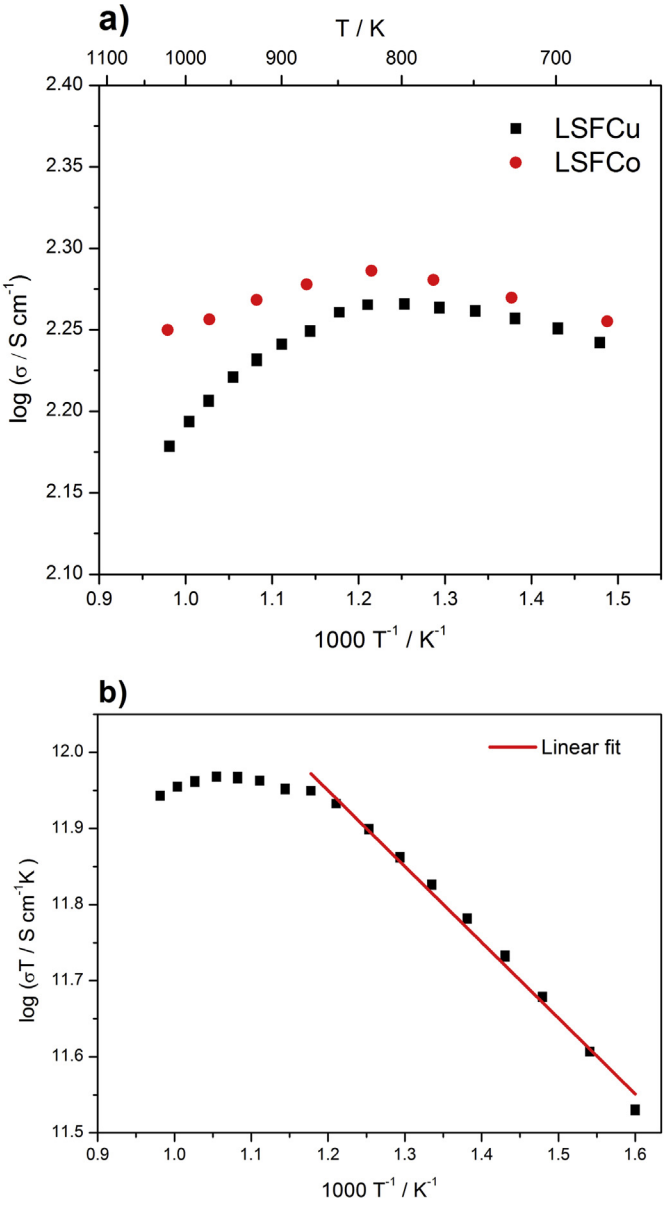

Fig. 6. a) Temperature dependence of LSFCu and LSFCo conductivities, b) Arrhenius plot of LSFCu.

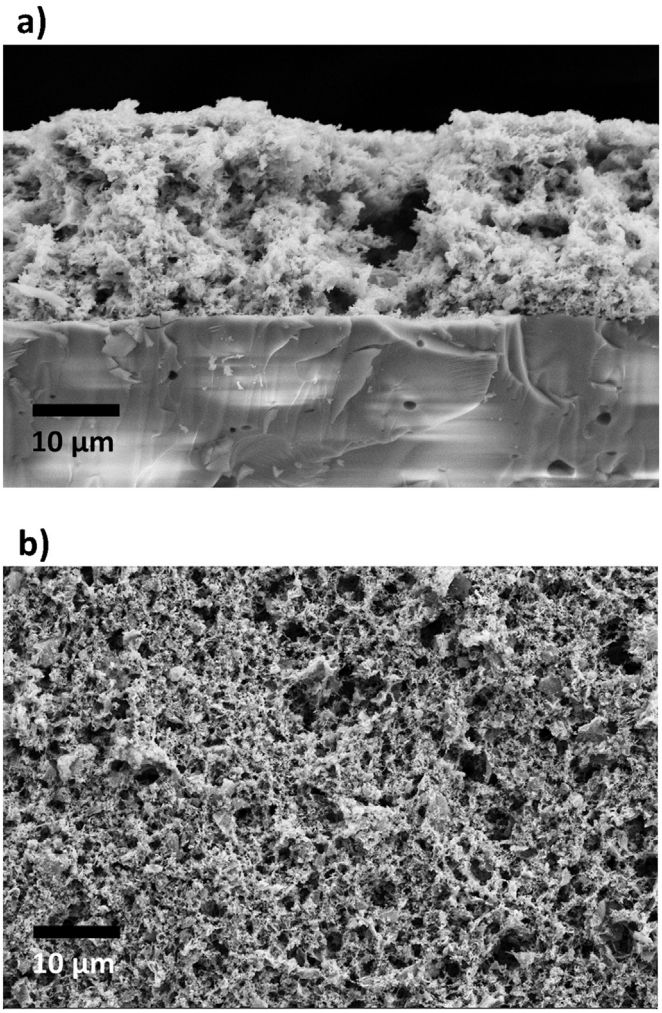

Fig. 7. SEM micrographs of LSFCu|LSGM half cell: a) cross-section, b) top view.

Both SIMS and SEM/EDX analyses indicate that Cu diffusion is present and confined in the more superficial region of LSGM while Co diffusion, proceeding mainly through the grain boundaries, penetrates more deeply into the LSGM matrix.

A performing cathode, apart from having very good activity for oxygen reduction, should be stable in oxidizing environment and have a high electronic conductivity (>100 S cm^{-1}). The substitutions of the trivalent La with divalent Sr ions in the A-site and that of Fe(III) with Cu(II) in the B-site affect the vacancy generation behavior and the electrical conductivity [27]. The temperature dependence of the electrical conductivity of LSFCu in air was measured and compared to that of LSFCo as reported in Fig. 6. Both compounds exhibited a thermally activated semiconducting behavior, due to a polaron hopping mechanism, and a typical metallic behavior above 550 °C. For both materials, the maximum conductivity value ($1.93 \cdot 10^2$ and $1.84 \cdot 10^2$ S cm^{-1} for LSFCo and LSFCu, respectively) was recorded at $T = 550$ °C. The LSFCu activation energy, derived from the Arrhenius plot shown in Fig. 6b, was 0.086 eV in the temperature range 350–575 °C, comparable to the value 0.11 eV reported in the literature for a similar compound, $La_{0.6}Sr_{0.4}Fe_{0.8}Cu_{0.2}O_{3-\delta}$ [23].

The electrochemical properties of LSFCu as cathode for LSGM have been assessed by two-electrode impedance to investigate the kinetics of the oxygen reduction reaction (ORR) and compare the results with those previously reported for the widely studied LSFCo. The adhesion between the cathode and electrolyte was investigated by SEM. Fig. 7 shows SEM micrographs of an LSFCu|LSGM half cell: cross-section (a) and top view (b). It reveals a good adhesion between cathode and electrolyte and proper porous microstructure of LSFCu. EIS experiments were carried out at various temperatures in synthetic air. Fig. 8 shows the Nyquist plots of LSFCu|LSGM|LSFCu and LSFCo|LSGM|LSFCo symmetric cells at different temperatures (Fig. 8a) and the corresponding Bode plots (Fig. 8b). The measured data were plotted in the complex plane and fitted to an equivalent circuit from which the ASR values reported in Fig. 8c were deduced. The equivalent circuits reported in the inset of Fig. 8a consisted of a resistance (R_{ohm}) in series with an inductance (L) and two equivalent circuit parameters (ECPs) in series attributed to two different mechanisms involved in the ORR. R_{ohm}, corresponding to the intercept at high frequency with the real axis, is the total ohmic contribution, R_1, corresponding to the high frequency arc, is the resistance ascribed to the charge transfer process, and R_2,

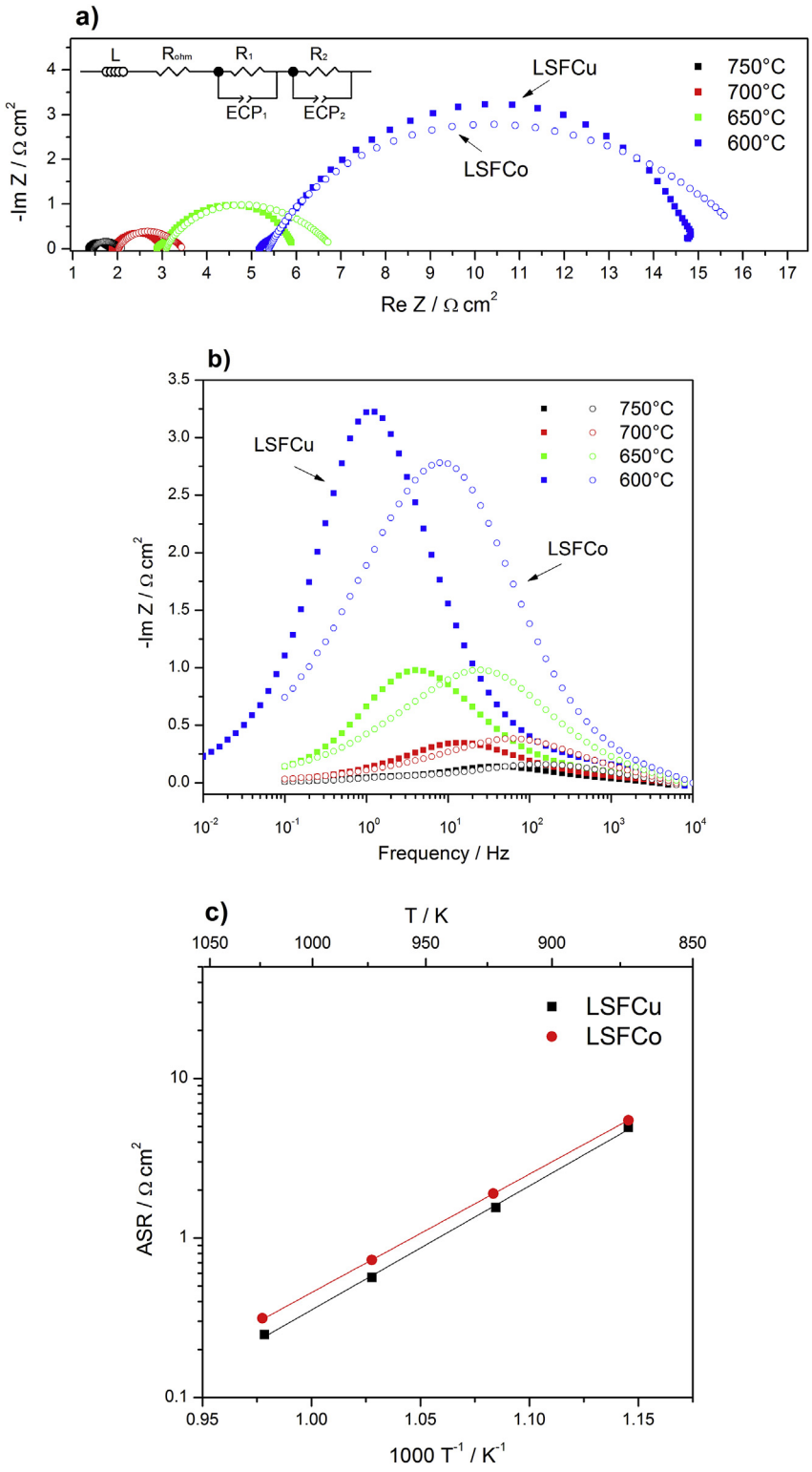

Fig. 8. a) Nyquist plots of LSFCu|LSGM|LSFCu and LSFCo|LSGM|LSFCo symmetric cells at different temperatures with the equivalent circuit, b) corresponding Bode plots; c) area specific resistance (ASR) versus the inverse of temperature.

corresponding to the low frequency arc, is attributed to oxygen adsorption and desorption on the electrode surface and it corresponds to the highest peak in the Bode plot (Fig. 8b) [28]. The height of the peaks of LSFCu and LSFCo in the Bode diagrams are comparable which means that the resistance value are similar, even if the LSFCo peaks are slightly shifted towards higher frequencies. This feature may be ascribed to a faster exchange of oxygen on the surface, related to the larger number of oxygen vacancies in LSFCo due to the larger charge imbalances in the A site of LSFCo stoichiometry [27].

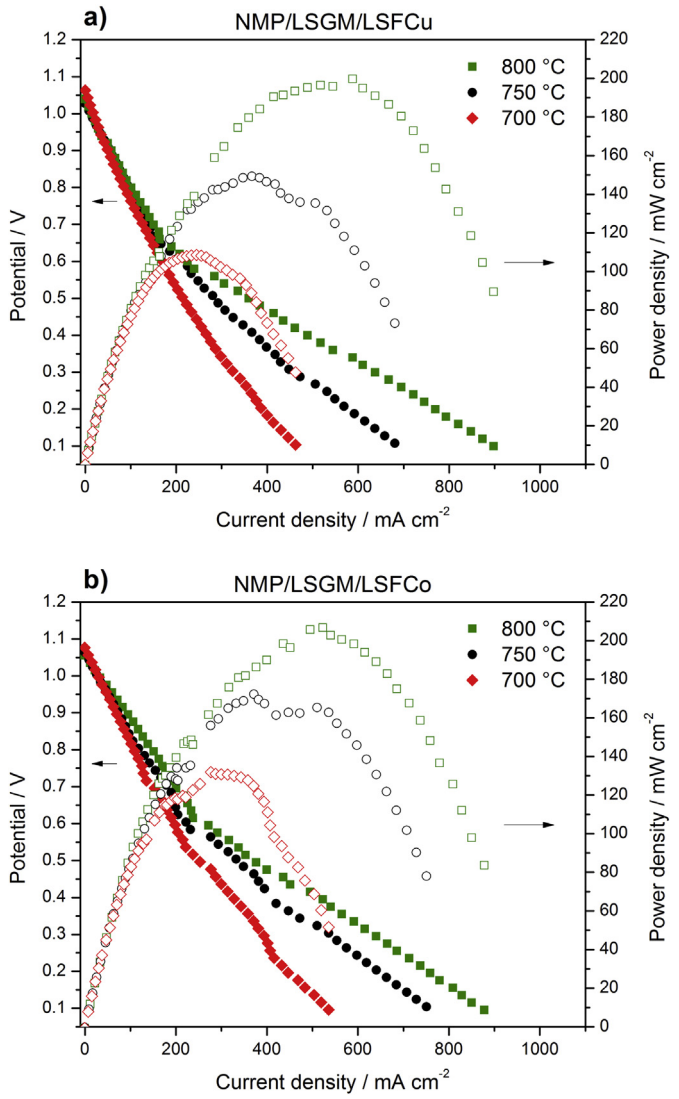

Fig. 9. *I–V* and power density curves of: a) LSFCu and b) LSFCo fuel cells at different temperatures using dry H_2.

The temperature dependence of the area specific resistance (ASR) values, derived from the polarization resistance (R_p), of LSFCu and LSFCo is shown in Fig. 8c. Data show no substantial difference between the two materials being, for instance, 0.25 Ω cm^2 vs 0.31 Ω cm^2 at 750 °C for LSFCu and LSFCo, respectively. The activation energies (E_a) for cathode polarization derived from the Arrhenius equation were 1.54 eV and 1.47 eV for LSFCu and LSFCo, respectively.

Single cells were fabricated using a previously reported Ni-modified perovskite anode (NMP) [27,28]. Fig. 9a and b shows the *I–V* and power density curves of NMP|LSGM|LSFCu and NMP|LSGM|LSFCo recorded using hydrogen as fuel and static air at the cathode at 700, 750 and 800 °C. Table 1 reports the measured values of open-circuit voltage (OCV) and maximum power density (P_{max}), together with the ohmic (R_{ohm}) and the electrode polarization (R_{pol}) resistances derived from EIS measurements at OCV. OCV values were always above 1 V at all investigated temperatures. Maximum power densities (P_{max}) at 800 °C were about 200 mW cm^{-2} for both cells. Although at lower temperatures the power outputs of LSFCo-based cells were slightly larger than those of LSFCu based cells probably because of the larger polarization resistance, the substitution of cobalt with copper does not appear to compromise the electrode performance.

Table 1
Performance of fuel cell tests of LSFCu and LSFCo based button cells in H_2 at different temperatures.

Temperature (°C)	LSFCu			LSFCo		
	800	750	700	800	750	700
OCV (V)	1.040	1.054	1.067	1.057	1.064	1.077
P_{max} (mW cm^{-2})	200	150	109	207	172	132
R_{ohm} (Ω cm^2)	0.57	0.72	0.91	0.65	0.76	0.97
R_{pol} (Ω cm^2)	0.31	0.58	1.3	0.23	0.28	0.46

4. Conclusions

Perovskite-type LSFCu oxide was synthesized and characterized as a novel "cobalt-free" cathode for LSGM. Interdiffusion between LSFCu and LSGM with formation of a solid solution was observed above 1100 °C. However, different to what it is observed in the case of Co containing cathodic material, where Co diffusion proceeds through grain boundaries into LSGM, Cu diffusion is mainly confined to superficial area as demonstrated by SIMS and EDX analyses.

The conductivity varied from 184 to 150 S cm^{-1} in the IT range (550–750 °C) demonstrating that LSFCu has suitable electrical property for cathode applications. The electrochemical performances measured in symmetrical and single cells were similar to those of the more widely investigated LSFCo. All these results make of LSFCu a potential candidate for application in LSGM based IT-SOFCs.

Acknowledgments

The financial support and collaboration of Consorzio Interuniversitario Nazionale per la scienza e Tecnologia dei Materiali and of the Lombardy Region of 13-11-2012 (Project "Ferriti di lantanio per nuove Fonti di Energia", Ferriti-NFE) and of Fondazione Roma and of the Italian Ministry for Education, University and Research (PRIN-2010-2011–Prot. 2010KHLKFC) are gratefully acknowledged.

References

[1] H.U. Anderson, Solid State Ionics 52 (1992) 33–41.
[2] Y. Takeda, R. Kanno, M. Noda, Y. Tomida, O. Yamamoto, J. Electrochem. Soc. 134 (1987) 2656–2661.
[3] J. Mizusaki, Solid State Ionics 52 (1992) 79–91.
[4] C. Lee, S.W. Baek, J. Bae, Solid State Ionics 179 (2008) 1465–1469.
[5] L.W. Tai, M.M. Nasrallah, H.U. Anderson, D.M. Sparlin, S.R. Sehlin, Solid State Ionics 76 (1995) 259–271.
[6] L.W. Tai, M.M. Nasrallah, H.U. Anderson, D.M. Sparlin, S.R. Sehlin, Solid State Ionics 76 (1995) 273–283.
[7] J.N. Kuhn, U.S. Ozkan, Catal. Lett. 121 (2008) 179–188.
[8] Z.P. Shao, S.M. Haile, Nature 431 (2004) 170–173.
[9] E.A. Kotomin, Y.A. Mastrikov, M.M. Kuklja, R. Merkle, A. Roytburd, et al., Solid State Ionics 188 (2011) 1–5.
[10] T. Ishihara, H. Matsuda, Y. Takita, Solid State Ionics 79 (1995) 147–151.
[11] N. Yang, A. D'Epifanio, E. Di Bartolomeo, C. Pugnalini, A. Tebano, G. Balestrino, S. Licoccia, J. Power Sources 222 (2013) 10–14.
[12] X.C. Lu, J.H. Zhu, J. Electrochem. Soc. 155 (2008) B494–B503.
[13] N. Sakai, T. Horita, K. Yamaji, M.E. Brito, H. Yokokawa, et al., J. Electrochem. Soc. 15 (2006) A621–A625.
[14] R. Pelosato, I. Natali Sora, V. Ferrari, G. Dotelli, C.M. Mari, Solid State Ionics 175 (1–4) (2004) 87–92.
[15] J. Larminie, A. Dick, Fuel Cell Systems Explained, second ed., Wiley, West Sussex, UK, 2003.
[16] J.E. Hong, T. Inagaki, S. Ida, T. Ishihara, Int. J. Hydrogen Energy 36 (2011) 14632–14642.
[17] B. Liu, W. Guo, F. Chen, C. Xia, Int. J. Hydrogen Energy 37 (2012) 961–966.

[18] J. Wackerl, T. Koppitz, D.H. Peck, S.K. Woo, T. Markus, J. Appl. Electrochem. 39 (2009) 1243–1249.
[19] U.F. Vogt, P. Holtappels, J. Sfeir, J. Richter, S. Duval, et al., Fuel Cells 9 (2009) 899–906.
[20] I. Natali Sora, T. Caronna, F. Fontana, C.D. Fernandez, A. Caneschi, et al., J. Solid State Chem. 191 (2012) 33–39.
[21] G. Coffey, J. Hardy, O. Marina, L. Pederson, P. Rieke, et al., Solid State Ionics 175 (2004) 73–78.
[22] K. Yasumoto, Y. Inagaki, M. Shiono, M. Dokiya, Solid State Ionics 148 (2002) 545–549.
[23] Q.J. Zhou, L. Xu, Y.J. Guo, D. Jia, Y. Li, et al., Int. J. Hydrogen Energy 37 (2012) 11963–11968.
[24] M. Lo Faro, V. Antonucci, P.L. Antonucci, A.S. Arico, Fuel 102 (2012) 554–559.
[25] M. Lo Faro, A.S. Arico, Int. J. Hydrogen Energy 38 (2013) 14773–14778.
[26] I. Natali Sora, F. Fontana, R. Passalacqua, C. Ampelli, S. Perathoner, G. Centi, F. Parrino, L. Palmisano, Electrochim. Acta 109 (2013) 710–715.
[27] N. Lakshminarayanan, H. Choi, J.N. Kuhn, U.S. Ozkan, Appl. Catal. B Environ. 103 (2011) 318–325.
[28] A. Esquirol, N.P. Brandon, J.A. Kilner, M. Mogensen, J. Electrochem. Soc. 151 (2004) A1847–A1855.